THE JOURNAL OF PHYSICAL CHEMISTRY C

Article

pubs.acs.org/JPCC

Molecular Structure and Dynamics in Thin Water Films at Metal Oxide Surfaces: Magnesium, Aluminum, and Silicon Oxide Surfaces

Anh Phan,[†] Tuan A. Ho,[†] D. R. Cole,[‡] and A. Striolo*[,†]

[†]School of Chemical, Biological and Materials Engineering, University of Oklahoma, Norman, Oklahoma 73019, United States

[‡]School of Earth Sciences, Ohio State University, Columbus, Ohio 43210, United States

ABSTRACT: All-atom equilibrium molecular dynamics simulations were employed to investigate the structural and dynamical properties of interfacial water on the magnesium oxide surface. The solid support was modeled utilizing two different formalisms, both based on the CLAYFF force field. In one case, the atoms in the MgO substrate are allowed to vibrate, whereas in the other they are maintained rigid. The properties of water within the thin film are assessed in terms of density profiles in the direction perpendicular to the substrate as well as along planes parallel to the substrate, in-plane radial distribution functions, density of hydrogen bonds, residence times in contact with the substrate, and orientation distribution of interfacial water molecules. The contact angle for a small droplet on various substrates (MgO, SiO_2, Al_2O_3) was also calculated and compared with experimental observations. On MgO, the substrate in which the atoms are maintained fixed is the one that most closely reproduces experimental contact angles. This contrasts with results on other substrates, for example, silicon dioxide, on which the vibrations of the solid atoms were found to be useful for better predicting experimental observations. These differences suggest that proper force-field validation is necessary before investigating the structure of interfacial water on solid substrates. In the case of MgO, our analysis suggests that the vibrations of the solid atoms yield atomic-scale roughness. This, in turn, causes water molecules to spread on the substrate. A brief comparison of water properties on MgO, alumina, and silica is provided.

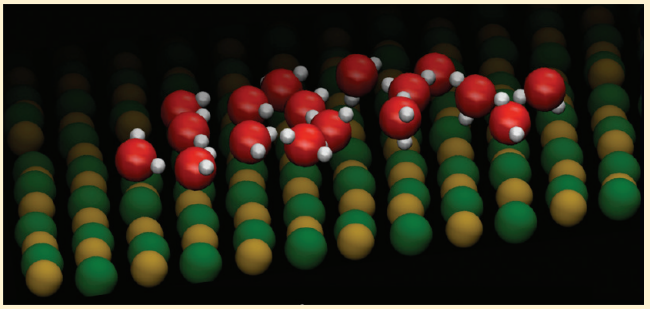

INTRODUCTION

The properties of water at solid−liquid interfaces play an important role in ion adsorption/desorption processes on solid substrates, diffusion of ions in nanopores, biological membranes, and ion channels.[1−5] It is known that structural and dynamical properties of interfacial water are strongly affected by the solid substrate characteristics, in general, yielding different behavior compared to that observed in the bulk.[6] One interface that receives significant attention is that between liquid water and metal oxides, which is crucial for a variety of industrial and environmental processes. Many oxide surfaces are used either as catalysts or as support for heterogeneous metal catalysts.[7,8] Interfacial water may in some cases improve the catalytic properties for those materials. In addition, water−mineral oxide chemistry is thought to determine hydrodynamic properties and reactivity in the earth subsurface.[9−12]

Magnesium oxide (MgO) is used as support for metal catalysts and high-temperature superconductors. It also provides a catalyst in its own right, occurs as the mineral periclase in a number of geological systems, and is a fundamental component of many minerals found in the subsurface. Because the MgO surface is well-characterized by both computational[13−15] and experimental efforts,[16] it is a widely used model system for investigating interfacial processes. Several experimental[17−22] and theoretical[23−26] studies have investigated the properties of the water/MgO interface. Scamehorn et al.[27] studied water adsorption on a three-layer (001) MgO film using density functional theory (DFT) at the Hartree−Fock level. Minot et al.[28] employed DFT to study ice filling the interspace between MgO (100) layers. It was found that water molecules close to the interface can dissociate under high pressure.

McCarthy et al.[29] studied structure and dynamics of an isolated water molecule as well as those of water multilayers on a perfect MgO (001) surface, identifying the most favorable adsorbate/surface geometry. Ab initio potential energy results were then used to parametrize atomistic simulations, implemented to determine the density profiles and the probability distributions of angular orientation for interfacial water molecules in a thin supported film.

To complement these early results, we employ here extensive all-atom equilibrium molecular dynamics (MD) simulations to investigate the structure of water molecules within thin films supported on MgO. In the case of SiO_2, it was found that accounting for atomic vibrations in the solid substrate is essential for capturing correctly the dynamics of interfacial water,[30−32] thereby supporting the contention that considering a substrate as completely immobile might lead to distortions in

Received: January 19, 2012
Revised: May 24, 2012
Published: May 29, 2012

   dx.doi.org/10.1021/jp300679v | J. Phys. Chem. C 2012, 116, 15962−15973

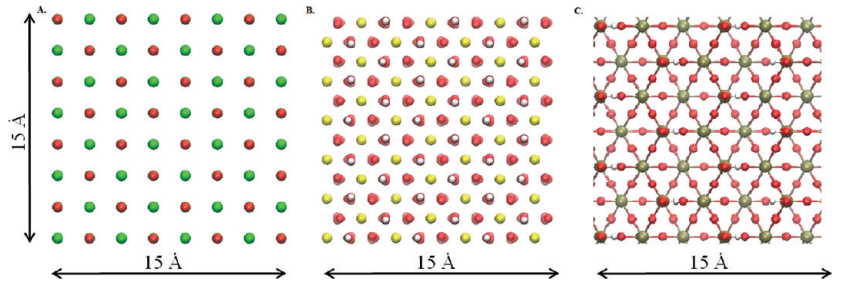

Figure 1. Top view of the magnesium oxide substrate used for the simulations reported here (left panel), of the fully hydroxylated alumina (middle panel), and of the low−OH-density hydroxylated silica (right panel) used in our prior works.[8,30,34,49] Green, yellow, tan, red, and white spheres represent magnesium, aluminum, silicon, oxygen, and hydrogen atoms, respectively. The crystal structure of MgO is described as face-centered-cubic with six coordinated oxygen and magnesium atoms. The crystal structure of hydrated α-Al_2O_3 (0001) consists of aluminum atoms surrounded by six oxygen atoms, which yield a dense hexagonal packing. Hydrogen atoms are located at three specific positions bonding with oxygen atoms. For silica, all silicon atoms that are part of an incomplete tetrahedral were removed, and one silicon atom is bonded to nonbridging oxygen atoms, which were saturated with hydrogen atoms.[39]

the predicted structure and dynamics of interfacial water.[33] Here we compare the results obtained when MgO is treated as rigid versus when its atoms are allowed to vibrate, finding better reproduction of experimental contact angles when the MgO atoms are maintained rigid. The resultant properties of interfacial water are compared with those previously reported for water on alumina and silica dioxide.[30,34]

SIMULATION METHODOLOGY AND DETAILS

The MgO surface was represented as a solid film of thickness 10.51 Å. A theoretical study indicates that this is the thinnest film in which the charge density of the atoms in the center layer is similar to those found in the bulk material.[14,27] Previous studies, both experimental[16,35−37] and theoretical,[14] have suggested that no significant surface reconstruction or relaxation occurs upon cleavage of a MgO crystal along the (001) plane. Therefore, the symmetry of the bulk is retained in the solid substrate. The plane group used to describe the (001) surface is derived from the space group *Fm*3*m*. The solid MgO substrate is aligned parallel to the *XY* plane of the simulation box, and a thin water film is prepared along the *Z* direction, following the procedures of our prior investigations.[30,34,38,39] The simulations were carried out in orthorhombic simulation boxes of constant volume. The *X* and *Y* dimensions of the simulation boxes reflect the periodicity of the solid crystalline substrate with values of 10.5 nm. The *Z* dimension was set to 16.27 nm.

The CLAYFF force field was implemented to simulate MgO.[33] To prevent vibrations of the solid atoms (nonvibrating MgO), we froze all atoms in the substrate. To allow vibrations of the atoms in the substrate (vibrating MgO), we kept the Mg and O atoms within the atomic layer furthest from the interface frozen, whereas all other atoms were allowed to move as prescribed by CLAYFF. In Figure 1, the top view of the MgO surface (left panel), studied here, is compared with the fully hydroxylated alumina (middle panel) and silica surfaces (right panel) used in our previous simulations.[30,34] The crystal structure of MgO (001) is cubic with octahedral Mg and O ions. By comparison, the oxygen ions on the (0001) crystallographic face of corundum α-Al_2O_3 surface yield a hexagonal close-packed structure with aluminum ions filling two-thirds of the octahedral interstices. The silica surface shown in Figure 1 is obtained from the β-cristobalite SiO_2 crystal.[30,39]

The rigid SPC/E model was used to simulate water.[40] The model is known to reproduce reasonably well the structure and dynamics of the bulk liquid under ambient conditions. Although CLAYFF was derived for solid substrates interacting with the SPC model of water, using either the SPC/E or the SPC models was found to yield no difference at the water−silica interface.[30] In the present work, the SPC/E water bonds and angles were kept fixed by employing the SETTLE algorithm.[41] We simulated ∼15 000 water molecules to create a thin water film of 45 Å thickness on MgO. As the *Z* dimension of the simulation box was 16.27 nm, and as the solid substrate thickness was 10.51 Å, an empty gap remains between the thin film and the periodic image of the solid substrate, as in our prior studies.[30,34,39]

Nonbonded interactions were modeled by means of dispersive and electrostatic forces. The electrostatic interactions were modeled by the Coulombic potential. Dispersive interactions were modeled with a 12−6 Lennard-Jones (LJ) potential. The LJ parameters for unlike interactions were determined by Lorentz−Berthelot mixing rules[42] from the values of like components. The cutoff distance for all interactions was set to 9 Å. Long range corrections to electrostatic interactions were treated using the particle mesh Ewald (PME) method.[43]

All simulations were performed in the canonical ensemble (NVT), where the number of particles (N), the simulation volume (V), and the temperature (T) were held constant. T was fixed at 300 K and controlled by a Nosé−Hoover thermostat[44,45] with a relaxation time of 100 fs. Periodic boundary conditions were applied in the three directions. The equations of motion were solved using the simulation package GROMACS[46,47] by implementing the leapfrog algorithm[48] with time step of 1.0 fs. Total simulation time is 3 ns. Data analysis was conducted over the last 2 ns of the simulations, after 1 ns of equilibration was completed.

Additional simulations were carried out for computing contact angles, in which case 1000 water molecules were supported on the solid substrates for 5 ns.

RESULTS AND DISCUSSION

1. Contact Angle. It remains difficult to characterize the properties of a solid−water interface, in particular, when appropriate comparisons to experimental observations are attempted. Garde and coworkers found that water density fluctuations near a substrate are related to a number of

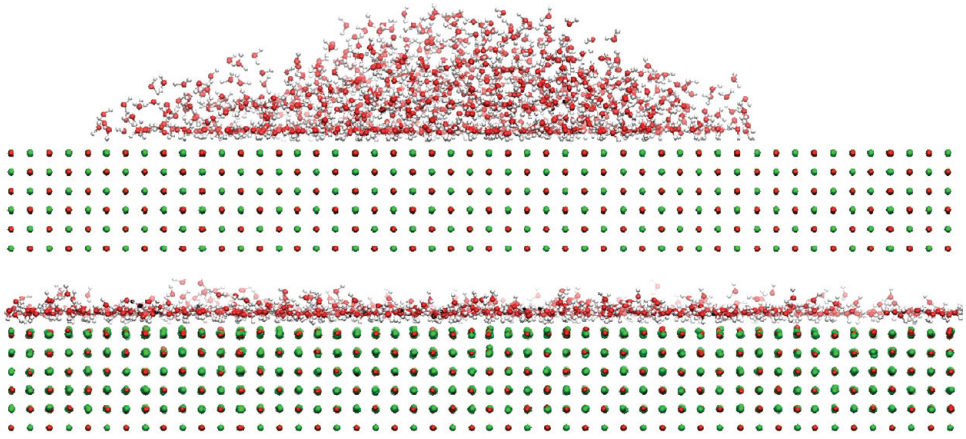

Figure 2. Representative simulation snapshots of a droplet of 1000 water molecules equilibrated on a nonvibrating (top panel) and a vibrating MgO surface (bottom panel). Red, white, and green spheres represent oxygen, hydrogen, and magnesium atoms, respectively.

macroscopic phenomena, including the adsorption free energy of several compounds on hydrophilic versus hydrophobic surfaces.[50] In general, however, the contact angle is one of the quantities that yields a straightforward comparison between experimental and simulation studies, despite a few known limitations (e.g., the simulated contact angle depends on the droplet size,[6] experimental data suggest that the dynamic contact angle is a more reliable quantification of surface hydrophobicity in some applications than the static contact angle,[51] the atomic-level morphology of a surface strongly affects the contact angle in heterogeneous surfaces,[52] and the static contact angle alone is not sufficient to characterize a surface toward macroscopic quantities such as hydrodynamic boundary conditions[53]).

We carried out simulations with 1000 water molecules placed on the substrates to quantify the contact angle for water on the model MgO surfaces considered. The snapshots obtained after 5 ns of simulation are shown in Figure 2 for a nonvibrating (top) and a vibrating MgO surface (bottom panel). In both cases, the water−MgO interactions are described by the CLAYFF force field.

When the atoms in the MgO surface are maintained rigid, the nanodroplet yields a well-defined shape. The simulated contact angle, obtained following the method proposed by Giovambattista et al.,[54] is ∼47° at 300 K and ∼56° at 293 K, which is in reasonable agreement with the experimental value of 58.1°.[55] Surprisingly, when the MgO surface atoms vibrate, water molecules spread, yielding a monolayer and suggesting that the surface is much more "hydrophilic" than reported by experiments. Because of the better agreement with experiments, the results in Figure 2 suggest that the CLAYFF force field could be used to simulate the water−MgO interface provided the solid atoms are not allowed to vibrate.

It remains to be understood why the vibration of the MgO atoms has such an important effect on the simulated water contact angle. It should be noted that the simulation started with a thin film of 1000 water molecules on the nonvibrating MgO surface yields a water droplet (i.e., the water molecules dewet the surface). It should also be pointed out that when simulations are conducted in the NVE ensemble (the energy is maintained constant while the temperature fluctuates) the contact angle observed on the rigid MgO substrate is comparable to the one obtained conducting the simulations in the NVT ensemble, provided that results are obtained when the system is at the same temperature.

In the force field implemented here, the atoms in the solid substrate are not bound to each other, and their vibrations are due to thermal fluctuations coupled to interactions with other atoms in the solid and in the interfacial liquid water. Although these modes of vibration are expected to be realistic, it is possible that describing the solid atoms as charged Lennard-Jones spheres does not fully capture the properties of the solid. However, it should be pointed out that the CLAYFF force field has been successful in reproducing experimental observations for a number of mineral substrate−water interfaces. An alternative explanation for the different contact angle might be related to effective temperature effects. (Preventing the solid atoms vibrations might effectively lower the temperature of the interfacial system.) However, in the NVT ensemble, all water molecules are maintained at the desired temperature.

To better understand the molecular reasons responsible for the different simulated contact angles when the MgO support is allowed to vibrate or not, we conducted additional simulations in the NVT ensemble. For these simulations, we used as the initial configuration for the solid substrate the final configuration obtained from simulating water on the vibrating MgO substrate (Figure 2, bottom). The simulations were then conducted maintaining the MgO atoms frozen. This substrate is characterized by atomic-scale roughness as the atoms move by less than ∼0.2 nm from their crystal positions. The 1000 water molecules simulated on this substrate were found to spread on it whether they were initially in a thin film or in a 3-D rectangular arrangement. Therefore, we conclude that allowing for the MgO atoms to vibrate induces atomic-scale roughness. It is this roughness that causes the water molecules to spread on the substrate yielding a contact angle larger than that observed experimentally.

Although the contact angle differed on nonvibrating versus vibrating surfaces, other interfacial water properties, such as density profiles away from the solid, radial distribution functions (RDFs), planar density distributions, hydrogen bond (HB) network, and residence times are similar within thin water films supported on the two surfaces, as discussed below. The orientation of water molecules within the first hydration layer, however, is found to depend on whether the solid substrate vibrates.

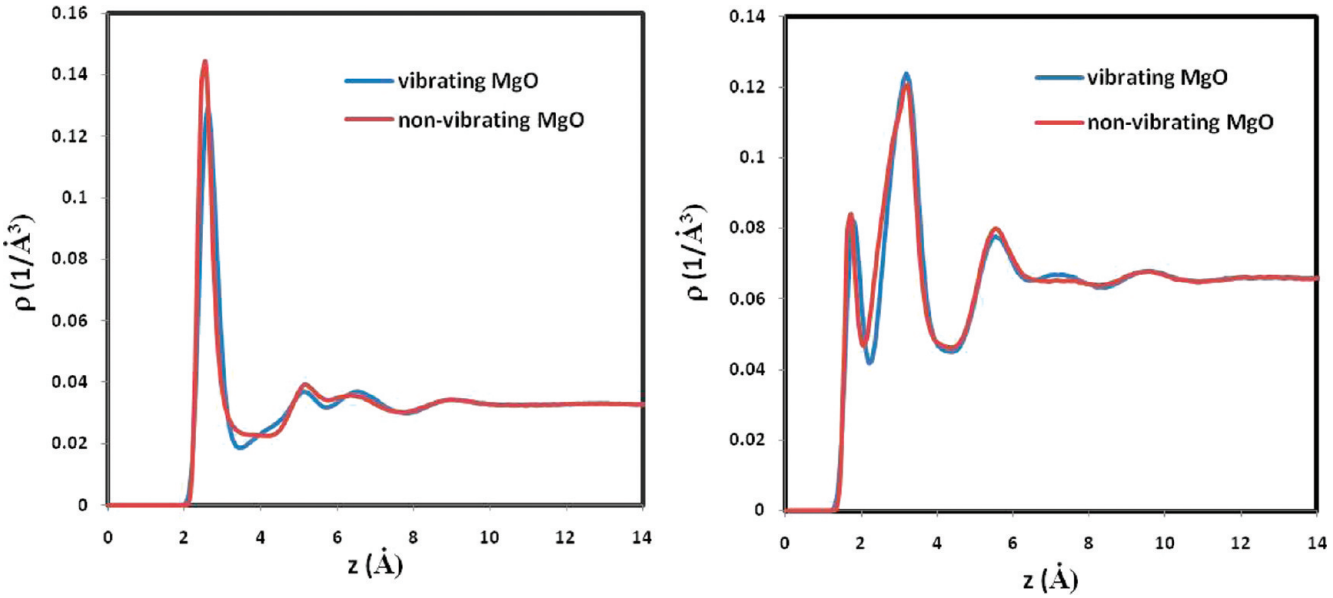

Figure 3. Oxygen (left panel) and hydrogen (right panel) atomic density profiles of water as a function of the vertical distance z from a vibrating (blue line) and a nonvibrating (red line) MgO surface.

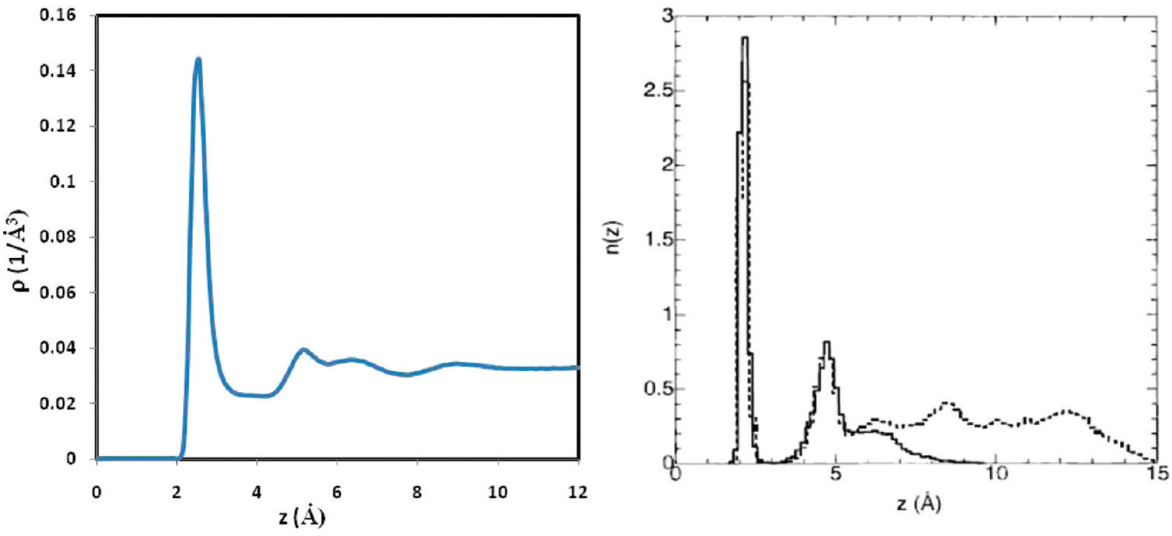

Figure 4. Oxygen atomic density profile as a function of distance z from the rigid MgO surface obtained in our simulation (left panel) and that reported by McCarthy et al.[29] (right panel). In the right panel, the number of water molecules simulated is either 64 (solid line) or 128 (dotted line). In the y axis, n (z) is the number of water molecules per MgO unit cell. The right panel is reproduced from ref 29.

2. Atomic Density Profiles. In Figure 3, atomic density profiles of water oxygen (left panel) and hydrogen atoms (right panel) are reported as a function of the distance from a nonvibrating (red lines) and a vibrating MgO surface (blue lines). For the rigid MgO surface, the reference (z = 0) corresponds to the top plane of magnesium and oxygen atoms in the solid substrate. For the vibrating surface, because surface atoms oscillate around their equilibrium positions, the averaged location of top layer atoms is considered as the reference.

The oxygen atomic density profiles (left panel) indicate the formation of a well-defined hydration layer at z = 2.55 Å on the nonvibrating as well as on the vibrating surface. The comparable intensity of these peaks and the similar profiles suggest that surface atom vibrations do not affect the water structure.

The results obtained for the hydrogen atomic density profiles presented in the right panel support the observation summarized in the previous paragraph. By comparing the density profiles of oxygen and hydrogen atoms, the orientation of water molecules can be also studied, as discussed in detail elsewhere.[30,34,38,53] Our results suggest that ∼60% of the water molecules found in the first hydration layer near MgO project one of their hydrogen atoms toward the solid substrate, whereas the remaining waters tend to maintain both OH bonds pointing away from the surface.

In Figure 4, the density profile for oxygen atoms of water obtained from our simulations on the nonvibrating MgO surface is compared to that reported by McCarthy et al.,[29] who also considered a nonvibrating MgO surface. McCarthy et al.[29] used the correlation-corrected periodic Hartree−Fock (PHF) theory to compute ab initio electronic structure energy data.

dx.doi.org/10.1021/jp300679v | J. Phys. Chem. C 2012, 116, 15962−15973

Table 1. Force-Field Parameters Implemented by McCarthy et al. and Those Implemented Herein

	force fields implemented by McCarthy et al.[29]				this work		
	A (kcal/mol)	B (Å^{-1})	C (kcal/mol) Å^6	q	D_o (kcal/mol)	R_o (Å)	q (e)
O_{water}	331 568	4.35	154	−0.82	0.1554	3.5532	−0.82
H_{water}	700	3.37	18	0.41	0	0	0.41
Mg_{surf}	22 645	4.24	1224	1.966	9.0298×10^{-7}	5.9090	1.05
O_{surf}	95 810	4.36	252	−1.966	0.1554	3.5532	−1.05

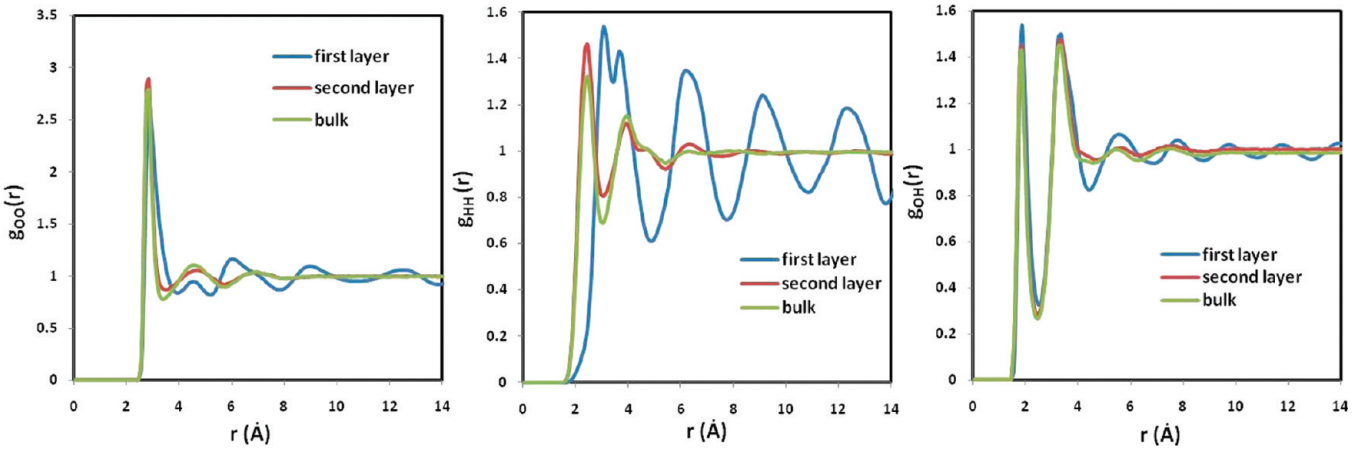

Figure 5. In-plane oxygen−oxygen radial distribution functions $g_{OO}(r)$ (a), hydrogen−hydrogen radial distribution functions $g_{HH}(r)$ (b), and oxygen−hydrogen radial distribution functions $g_{OH}(r)$ (c) within the first and second layers at the nonvibrating MgO surface. For comparison, data obtained for "bulk" water are also shown. For "bulk" water simulation results obtained in the center of the thin films simulated herein were used.

They then used the results to fit the parameters A, B, and C of a pairwise additive potential energy expression

$$V = \sum_{i<j} \left[\frac{q_i q_j}{r_{ij}} + A_{ij} \exp(-B_{ij} r_{ij}) - \frac{C_{ij}}{r_{ij}^6} \right] \quad (1)$$

The particle charges on the MgO ions were obtained by implementing a Mulliken population analysis of the PHF charge density results. The partial charges q obtained were +1.966 |e| and −1.966 |e| on magnesium and oxygen atoms, respectively. In eq 1, r is the distance and subscripts i and j denote different atoms.

In CLAYFF, the Lennard-Jones (12−6) potential is chosen to describe van der Waals interactions, which are augmented by electrostatic forces as described by the following expression

$$V = \sum_{i<j} \left\{ \frac{q_i q_j}{r_{ij}} + D_{o,ij} \left[\left(\frac{R_{o,ij}}{r_{ij}} \right)^{12} - 2 \left(\frac{R_{o,ij}}{r_{ij}} \right)^{6} \right] \right\} \quad (2)$$

In CLAYFF, the particle charges q are +1.05 |e| and −1.05 |e| on magnesium and oxygen, respectively. R_o and D_o are interaction parameters. The force-field parameters implemented by McCarthy et al. and those used in the present work are summarized in Table 1.

McCarthy et al.[29] simulated either 64 or 128 water molecules and reported the density profiles in terms of the number of water molecules per MgO unit cell (n). They found a well-pronounced first hydration layer at $z \approx 2.25$ Å from the substrate, which is in good agreement with our results. The intensity they reported for this first hydration layer, ∼2.8 water molecules per MgO unit cell, corresponds to an atomic density of ∼0.1524 (1/Å^3), which is slightly larger than that obtained from our simulations. This slight difference could be due to the larger number of water molecules considered in our simulations and to differences in the force fields implemented, but, in general, our results show good agreement with those reported by McCarthy et al.

More significant differences include a pronounced gap evidenced by the density profile proposed by McCarthy et al. in between the first and the second hydration layers, which is not present in our results, and a much more pronounced ratio between the density of the first hydration layer and the density far from the surface (at ∼1 nm) observed by McCarthy et al. than in our results. These details suggest that the force fields implemented by McCarthy et al. yield a slightly more structured hydration layer, which could affect the prediction of macroscopic phenomena such as hydrodynamic slip and macromolecular adsorption. Experimental scattering results are necessary for discriminating which of the results shown in Figure 4 is the most realistic.

3. In Plane Radial Distribution Functions. In-plane RDFs for oxygen−oxygen, hydrogen−hydrogen, and oxygen−hydrogen pairs are calculated to quantify the different structural properties within the first hydration layer compared with those observed for water molecules in the second hydration layer or in the bulk. For these calculations, water molecules within a thin water slab parallel to the surface are considered. The thickness (δz) of the slab is 1 Å in all cases, and the center of a slab corresponds to one of the peaks in the density profiles shown in Figure 3. The bulk is identified as the center of the thin interfacial water film ($z > 14$ Å).

In Figure 5, results of oxygen−oxygen (left), hydrogen−hydrogen (middle), and oxygen−hydrogen (right) RDFs are shown for water in the first layer, second layer, and in the bulk (data obtained on the nonvibrating MgO). The results for $g_{OO}(r)$ and $g_{OH}(r)$ obtained for different hydration layers do not show significant differences, although the data obtained in

dx.doi.org/10.1021/jp300679v | J. Phys. Chem. C 2012, 116, 15962−15973

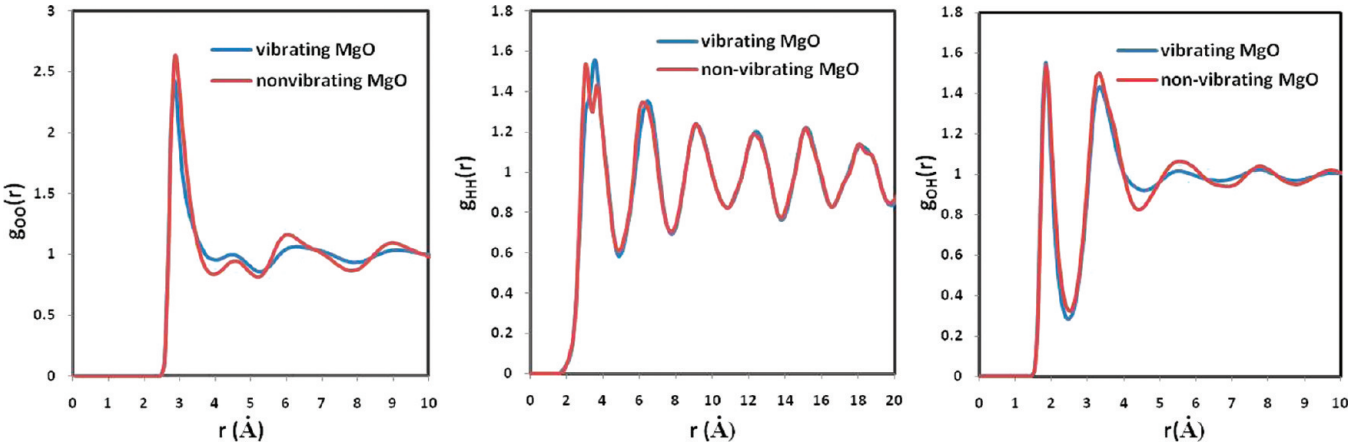

Figure 6. In plane oxygen−oxygen $g_{OO}(r)$ (a), hydrogen−hydrogen $g_{HH}(r)$ (b), and oxygen−hydrogen radial distribution functions $g_{OH}(r)$ (c) for water molecules within the first hydration layer on the vibrating and nonvibrating MgO surfaces.

the first hydration layer suggest a slightly more pronounced structuring of water within the first layer (see left panel). More pronounced differences are observed for g_{HH}. In particular, several pronounced peaks are observed in the $g_{HH}(r)$ data obtained within the first hydration layer, suggesting significant water orientational ordering. The results obtained for the second hydration layer are very similar to those obtained for bulk water, indicating that MgO surface perturbs the water structure only at short distances, in qualitative agreement with the density profiles in Figure 3. Data for g_{OH} do not seem to depend much on the layer position, although the water molecules in the first hydration layer show a slightly more ordered structure than those further away from the substrate.

To determine how surface atom vibrations affect the configuration of the first hydration layer, we computed the in-plane $g_{OO}(r)$, $g_{HH}(r)$, and $g_{OH}(r)$ (RDFs) obtained within the first hydration layer for vibrating and nonvibrating MgO surfaces. The results are compared in Figure 6. The position and intensity of peaks in all RDFs are the same for both surfaces, suggesting that the vibrations of surface atoms produce minimal differences in the structure of water within the first hydration layer compared with a rigid surface.

4. Hydrogen Bond Network. In Figure 7, we report the density profiles of water−water HBs as a function of the distance z from nonvibrating (red line) and vibrating (blue line) MgO surfaces. We employed the geometric criterion proposed by Marti[56] to identify a pair of hydrogen-bonded water molecules. The position of one HB is then defined as the midpoint between acceptor oxygen and donor hydrogen atoms. No significant differences are found among the results obtained when vibrating and nonvibrating MgO surfaces are compared. In both cases, our results indicate a high density of water−water HBs at z = 2.65 Å, corresponding to the position of the first hydration layer (Figure 3). This suggests that water molecules in the first hydration layer have a strong tendency of forming HBs among themselves. A second peak is also observed for water−water HBs at ∼0.6 nm from the substrate. This position corresponds to one pronounced density peak in the hydrogen density profile and also to a peak in the oxygen density profile (admittedly, the O peak is wide, see Figure 3). The correspondence of high density of water−water HBs and the density peaks in the direction perpendicular to the substrate suggests that many HBs are formed between water molecules belonging to the same hydration layer. This contrasts with

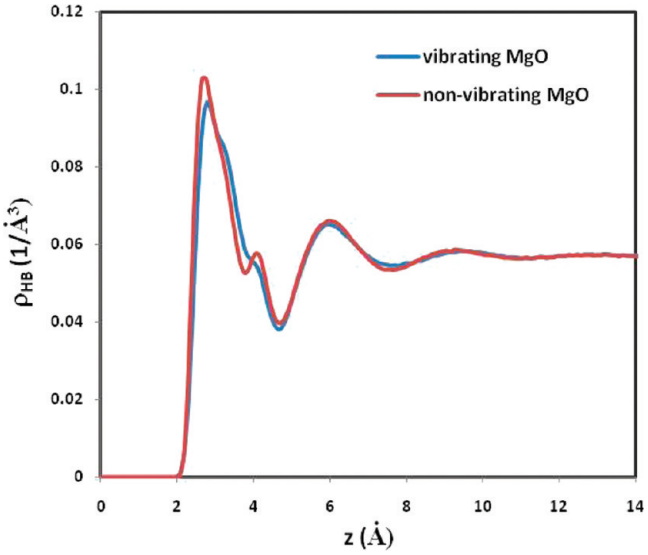

Figure 7. Density profiles of water−water hydrogen bonds as a function of distance from the vibrating (blue solid line) and the nonvibrating (red solid line) MgO surfaces.

results reported for example for water on silica.[39] At larger distances from the surface, bulk-like properties are quickly restored, again suggesting that MgO has a short-ranged effect on interfacial water.

5. In-Plane Density Distributions. To document the molecular structure of hydration water, we calculated the in-plane density distributions of oxygen and hydrogen atoms. In Figure 8, left panel, we present the in-plane density distribution of water oxygen atoms belonging to first oxygen peak. (See Figure 3 for peak position.) The high-density areas (green-orange spots) of the contour plot indicate the positions where the water oxygen atoms preferentially reside. These positions are on top of the magnesium atoms on the solid substrate. (See left panel in Figure 1.) The in-plane density distribution of the hydrogen atoms of water closest to the surface is shown in Figure 8, center panel. The positions of the high-density spots correspond to the position of oxygen atoms in the solid substrate, possibly a result of an attempt to form HBs. This water−solid interaction determines a preferential orientation of water molecules within the first hydration layer, reflected in the density profiles of Figure 3. The in-plane density distribution of

dx.doi.org/10.1021/jp300679v | J. Phys. Chem. C 2012, 116, 15962−15973

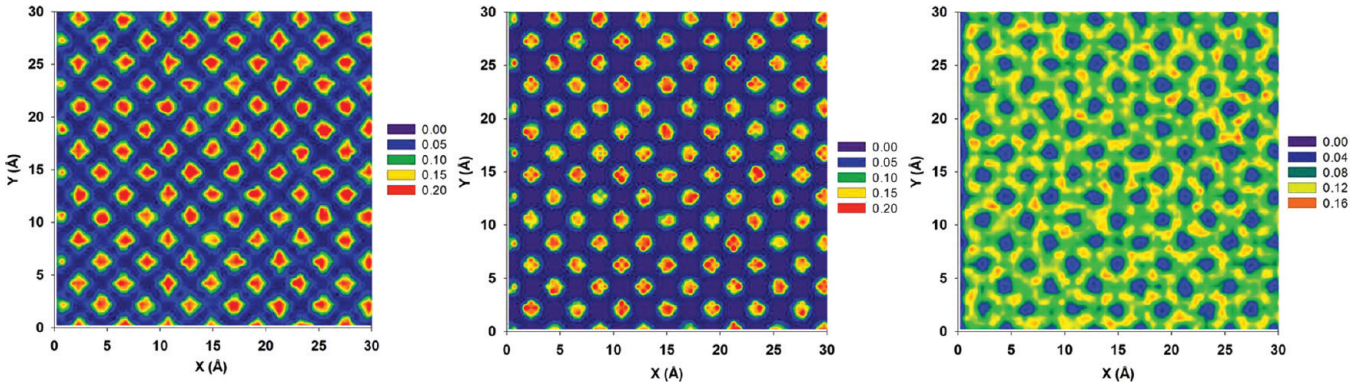

Figure 8. Surface density distributions of water oxygen atoms found in the first oxygen peak (left) and water hydrogen atoms found in the first (center) and the second hydrogen peaks (right) on the nonvibrating MgO surface. See Figure 3 for peak positions away from the surface. Densities are expressed in $1/Å^3$.

hydrogen atoms in the second layer away from the substrate is shown in Figure 8, right panel. The contour plot shows a pattern of green-orange circular-like areas distributed around blue spots regularly distributed on the surface. The positions of the blue areas (low hydrogen density) correspond to the position of the high-density locations observed for hydrogen atoms in the first layer (center panel). The distribution of water molecules in the first hydration layer (left panel), coupled to the water orientation dictated by the interaction with the surface (center panel), is responsible for the patterned distribution of hydrogen atoms shown in the right panel. The results just discussed were obtained on the nonvibrating MgO substrate. They are analogous to those obtained on the vibrating substrate (results not shown for brevity).

6. Residence Times and Hydrogen Bond Network. In Figure 9, we report the residence autocorrelation functions $C_R(t)$ for water molecules within the first hydration layer on the vibrating (blue line) and nonvibrating (red line) MgO surfaces. The residence autocorrelation function obtained for water molecules within a thin layer in the bulk region far from the surface (green line) is also shown for comparison. Following our prior procedures, the hydration layer was assigned a 1 Å thickness. The residence autocorrelation function can be used to quantify how long one water molecule remains in a specific layer. (For a discussion, see ref 39.) The faster the autocorrelation function decays, the shorter water molecules stay in a specific hydration layer.

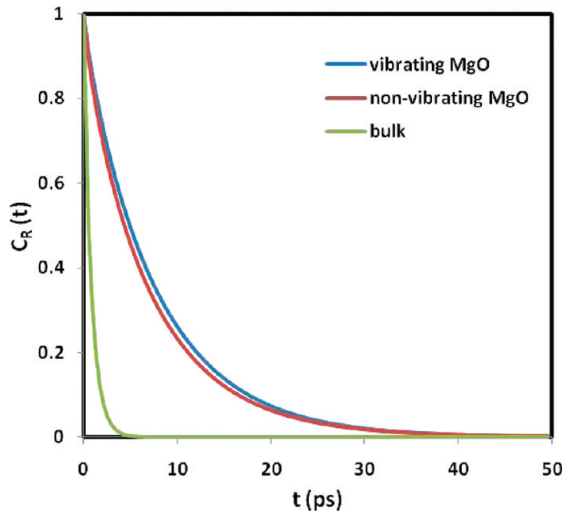

Figure 9. Residence autocorrelation functions $C_R(t)$ for water molecules within the first hydration layer on the vibrating (blue line) and on the nonvibrating MgO surface (red line). For comparison, the residence autocorrelation function for water molecules in a thin bulk layer is also shown (green line).

Comparing the residence autocorrelation functions $C_R(t)$ for water molecules within the first hydration layer with that of bulk water suggests that the closer water molecules are to the substrate, the longer they remain within a given layer. This result is consistent with data observed for many other substrates, especially when water molecules are attracted to the solid surface. The nearly identical features of $C_R(t)$ obtained for water molecules within the first hydration layer on both vibrating and nonvibrating surfaces suggest that the surface atom vibrations do not significantly affect the dynamical properties of interfacial water. This is surprising because in prior studies[30] it was found that surface atom vibrations significantly affect the dynamic properties of hydration water. In the case of silica, the effect was a function of the duration of surface water HBs. It is possible that on MgO the HBs between surface oxygen and water hydrogen atoms are not strongly affected by the vibrations of the solid atoms. It is also surprising that the residence autocorrelation functions $C_R(t)$ in Figure 9 decay faster for the nonvibrating compared to the vibrating MgO surface, although these differences are minimal and possibly due to statistical uncertainty. It is however possible that because the atomic-scale roughness induced by the vibration of the solid atoms promotes wetting, the individual water molecules are more strongly attracted to the vibrating surface, yielding slower decays in the residence autocorrelation function.

7. Orientation Distribution of Interfacial Water. In Figure 10, we present the probability distributions of the cosine of the polar angle formed between the dipole moment of water molecules and the surface normal vector for water on vibrating (left panel) and nonvibrating MgO substrates (right panel). We compare data obtained for water molecules within the first hydration layer (black lines) and those obtained for bulk water molecules (red dotted lines). The results show that interfacial water molecules on the vibrating surface have a much broader orientation distribution compared with those on the nonvibrating surface. This difference is probably related to the differences in atomic scale roughness of the two substrates. Interfacial water molecules adapt to the surface roughness

dx.doi.org/10.1021/jp300679v | J. Phys. Chem. C 2012, 116, 15962−15973

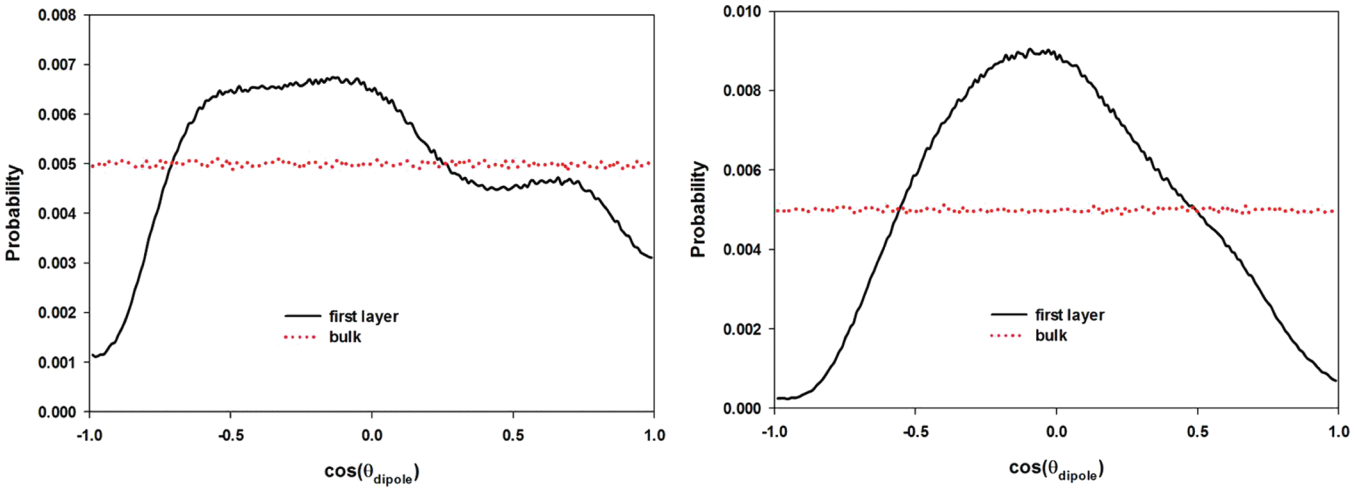

Figure 10. Probability distribution of $\cos(\theta_{dipole})$ within the first hydration layer on the vibrating (left) and nonvibrating (right panel) MgO surface. θ_{dipole} is the polar angle between the dipole moment of water molecules and the surface normal vector. Results for interfacial water (continuous black lines) are compared with those obtained for bulk water (dotted red lines).

typical of the vibrating MgO surface by adopting various orientations.

The results of Figure 10 complement the qualitative discussion regarding the orientation of interfacial water molecules presented in discussing Figure 3. The orientation distribution shown in Figure 10 is consistent with having ~60% of the interfacial water molecules oriented so that one of their OH vectors is projected toward the solid substrate while the other points away from it.

It is also worth pointing out that water molecules in the bulk do not show preferential orientation. The preferential orientation at the interface, which is also reflected in the HB network discussed in Figure 7, suggests that strong dipolar interactions exist between water and the MgO substrate whether the latter is vibrating or not. The model for water implemented herein cannot capture changes in the dipole moment of individual water molecules as they move from the bulk to an interface. Polarizable models are necessary for such investigations.[57]

8. Comparison with Other Substrates. We can gain further insight into solid−water interfacial behavior by comparing contact angles, density profiles, in-plane distributions as well as residence times for interfacial water obtained on the nonvibrating MgO, hydroxylated α-Al_2O_3, and hydroxylated SiO_2 surfaces. Results obtained on alumina and silica are discussed at length in our prior papers.[30,34,39] In the discussion below, the hydroxyl groups in the alumina and silica substrates are allowed to rotate (all other atoms are maintained rigid), whereas all atoms on MgO are rigid. These representations, based on our analysis, provide realistic descriptions of the three solid−liquid interfaces.

8.A. Contact Angles. We performed simulations for droplets of 1000 water molecules on the various substrates, as shown in Figure 11. The results demonstrate that water molecules wet alumina and silica, forming one hydration layer. The remaining water molecules form a droplet on top of the first hydration layer (Figure 11b,c). Conversely, a droplet is found on the MgO surface, as discussed in Section 1 (Figure 11a), without the formation of one hydration layer. Although this suggests that alumina and silica are more hydrophilic than MgO, the interesting result is that water molecules spread on alumina and silica, yielding one hydration layer, but then one water droplet

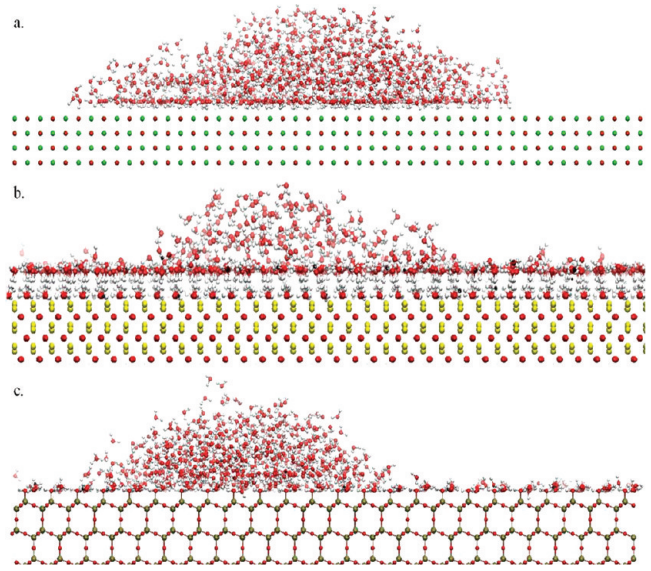

Figure 11. Representative simulation snapshots of droplets formed by 1000 water molecules supported on a nonvibrating MgO (a), hydroxylated alumina (b), and silica (c) surfaces. Red, white, green, yellow, and tan spheres represent oxygen, hydrogen, magnesium, aluminum, and silicon atoms, respectively.

forms on top of this layer (Figure 11b,c, side views, and Figure 12, top view). This observation is similar to the simulation results reported by Wang et al.,[58] who found, by MD simulations under ambient conditions, that after water molecules form one monolayer on an overall neutral, yet ionic substrate, additional "*water does not wet a water monolayer*". Under appropriate conditions, they found few HBs between the water molecules in the first hydration layer near the substrate and those within the water droplet, which explained the unexpected results, including the larger-than-expected contact angle for the water droplet supported onto the water monolayers. From an experimental point of view, Lutzenkirchen et al.[59] recently reported infrared data for thin water films on the sapphire c-plane [α-Al_2O_3 (0001)], which also suggest that the first hydration layer renders the surface hydrophobic to additional water molecules. Richardson et al.,[60]

dx.doi.org/10.1021/jp300679v | J. Phys. Chem. C 2012, 116, 15962−15973

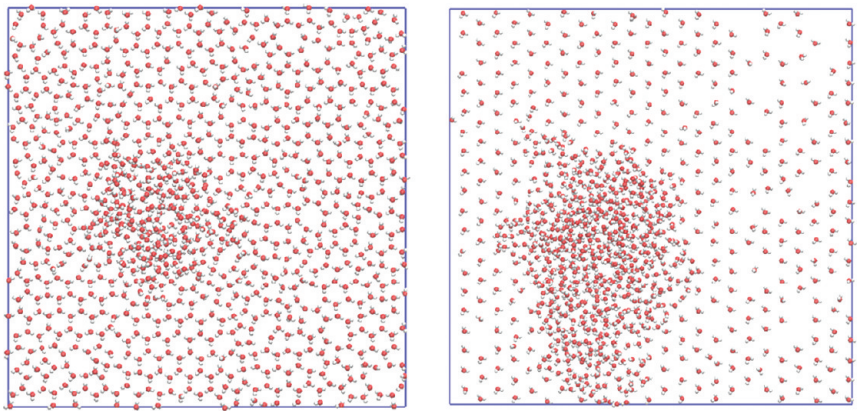

Figure 12. Top views of panels (b; Al_2O_3) and (c; SiO_2) (left and right panel, respectively) reported in Figure 11. The color code is analogous to that used in Figure 11. Only water molecules are shown for clarity.

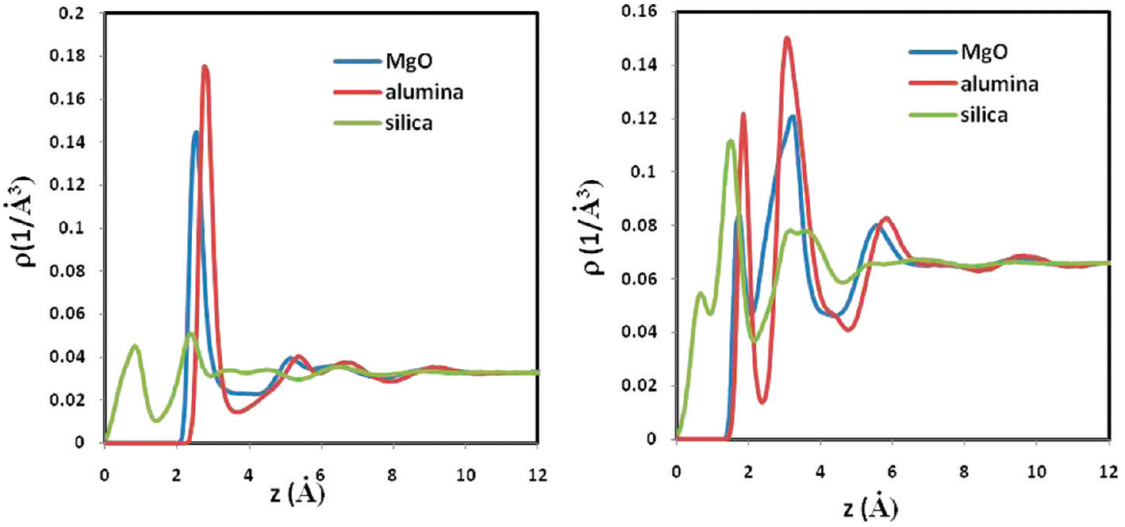

Figure 13. Atomic oxygen (left) and hydrogen (right) density profiles as a function of the vertical distance z from the nonvibrating MgO (blue), hydroxylated alumina (red), and hydroxylated silica (green) surfaces.

using FT-IR spectroscopy, reported qualitatively similar observations.

8.B. Atomic Density Profiles. In Figure 13, we report oxygen (left) and hydrogen (right panel) atomic density profiles on the MgO and hydroxylated α-Al_2O_3 and silica surfaces. Results on alumina and silica are from our prior publications.[30,34] The reference $z = 0$ for the alumina and silica surfaces is the plane formed by the oxygen atoms of the surface hydroxyl groups. The results for the oxygen atomic density profiles show that the intensity of the first oxygen water layer on MgO is comparable to that found on alumina and more intense than that found on silica. This is due to the different number of adsorption sites accessible to water on each surface. On MgO, water oxygen atoms adsorb on top of the Mg atoms (Figure 8), whereas on alumina and silica. interfacial water molecules form HBs with hydroxyl groups on the surfaces. The density of adsorption sites on MgO is comparable to that found on alumina (14 Mg atoms/nm^2 on MgO and 15 hydroxyl group/nm^2 on alumina[34]) but larger than that found on silica (4.54 hydroxyl groups/nm^2[30]). The higher density of adsorption sites is responsible for the larger density of water oxygen atoms found within the first hydration layer.

As explained above (Section 2) and in other detailed reports,[30,34,38,53] by comparing the intensity and position of the density profiles for oxygen and hydrogen atoms, it is possible to estimate semiquantitatively the orientation of interfacial water molecules, although detailed analysis such as that in Figure 10 is preferable for such characterizations.

8.C. In-Plane Density Distributions. In Figure 14, the in-plane density distributions of oxygen atoms in the first (A) and second (B) hydration layers on MgO (left panels), alumina (middle panels), and silica (right panels) surfaces are presented. Results of surface density distribution of oxygen atoms in the first hydration layer on alumina and in both layers on silica are from our prior studies.[30,34] The results suggest that water molecules occupy specific adsorption sites on each of the three surfaces. The distribution of water oxygen atoms within the first hydration layer reflects the atomic structure of the top layer of the solid substrate. On MgO, the location of water oxygen atoms corresponds to the surface Mg atoms, whereas on silica and alumina, water oxygen atoms are found near the surface hydrogen atoms, implying the formation of HBs between water molecules and the solid substrates.[61] Silica affects the structure of water molecules up to two hydration layers, whereas alumina and MgO affect only the first hydration layer. (Compare left and middle B panels to the right B panel in Figure 14.) These results are in agreement with the density profiles presented in Figure 13. However, note that the second hydration layer on

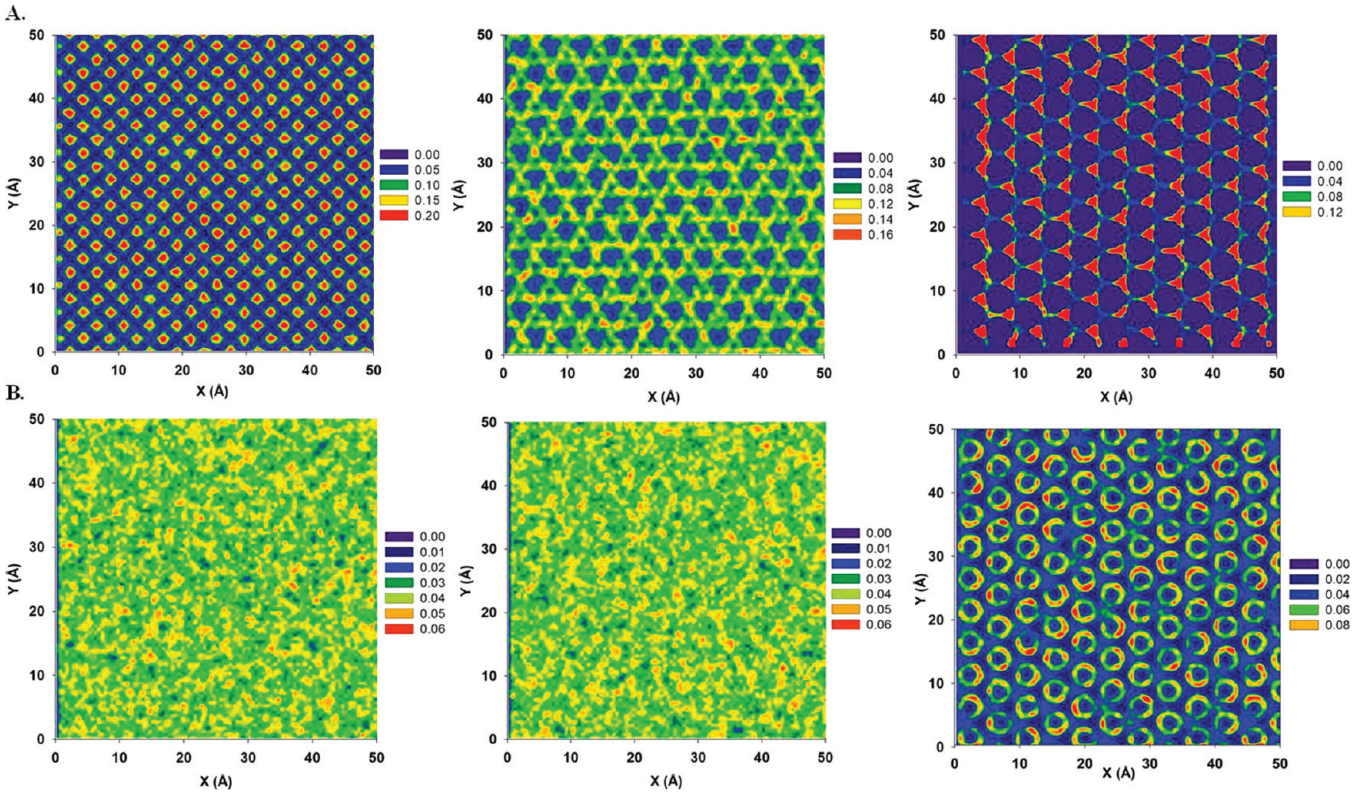

Figure 14. In-plane density distributions (parallel to the surface) for water oxygen in the first (A) and second (B) hydration layers formed on nonvibrating MgO (left panels), alumina (middle panels), and silica (right panels). See Figure 12 for the position of each hydration layer. Densities are expressed in $1/Å^3$.

silica is found at a z position that corresponds to approximately that of the first hydration layer on both MgO and alumina.

8.D. In Plane Radial Distribution Functions. In-plane oxygen−oxygen RDFs were calculated among the water molecules within the first hydration layer to gain better insight regarding the structural interfacial properties on the three substrates. For comparison, data for bulk water are also provided. The thickness (δz) of the first hydration layer was considered to be 1 Å in all cases. The results, shown in Figure 15, suggest that the water molecules within the first hydration layer on alumina have a structure similar to a dense liquid. Water structuring seems to increase on MgO. Some evidence of long-range ordering appears on silica, although on this substrate the first peak in the RDF is shifted to ∼0.5 nm because of the large distance between preferential adsorption sites on this substrate. (See the top right panel in Figure 14.) These results are a direct consequence of the structuring imposed by the solid substrates and are consistent with the in-plane density distributions shown in Figure 14A.

8.E. Residence Times and Hydrogen Bond Networks. In Figure 16, we report the results for the residence autocorrelation functions $C_R(t)$ obtained for water molecules within first and second hydration layers as well as in the bulk on MgO (left), alumina (middle),[34] and silica (right).[30] These results confirm that on these three substrates water molecules always remain within the first hydration layer longer than they do within the second layer and in the bulk region. The water molecules in the first hydration layer on alumina remain within the hydration layer much longer than those found within the first hydration layer either on MgO or on silica. The residence autocorrelation function for water molecules in the first layer

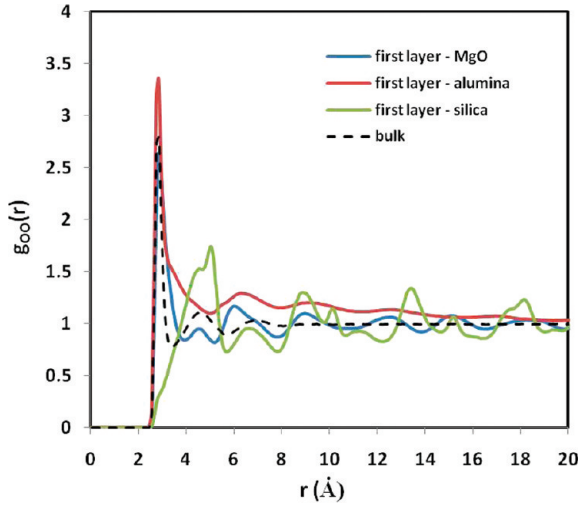

Figure 15. In plane oxygen−oxygen radial distribution functions, $g_{OO}(r)$, obtained within the first hydration layer on nonvibrating MgO (blue), alumina (red), and silica (green). For comparison, data for bulk water are also shown as black broken line.

on MgO decays more slowly than the corresponding one on silica. Water molecules reside within the second hydration layer on silica for longer times, on average, than they do on either MgO or alumina.

The dynamical properties of interfacial water depend strongly on the interactions between water molecules and the solid substrate as well as on those between different water molecules. Such interactions are often reflected on the HB network. In Figure 17, water−water HB density profiles are

dx.doi.org/10.1021/jp300679v | J. Phys. Chem. C 2012, 116, 15962−15973

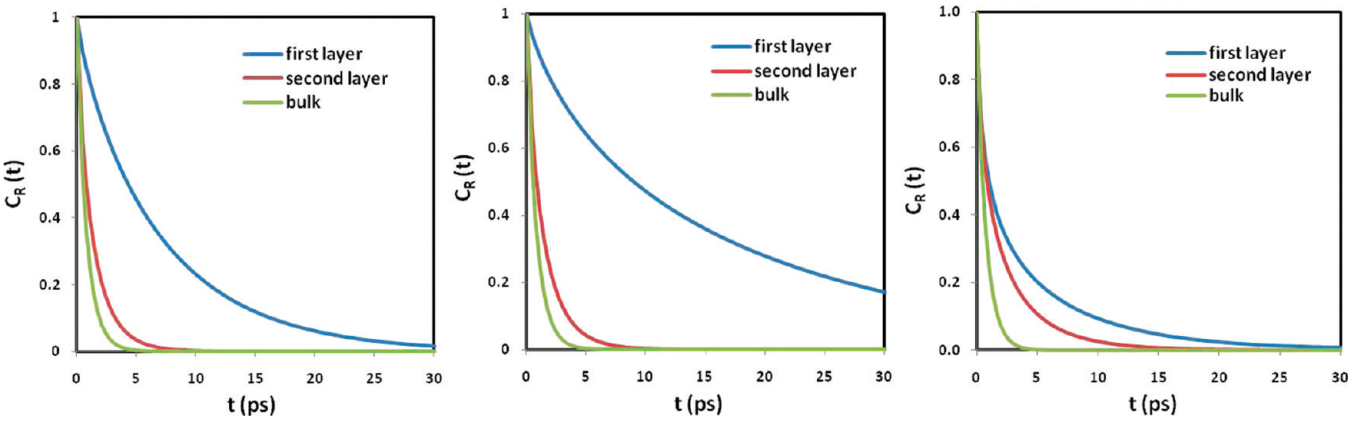

Figure 16. Residence autocorrelation functions $C_R(t)$ for water molecules within various interfacial layers on nonvibrating MgO (a), hydroxylated alumina (b), and hydroxylated silica (c). Data for bulk water are provided for comparison.

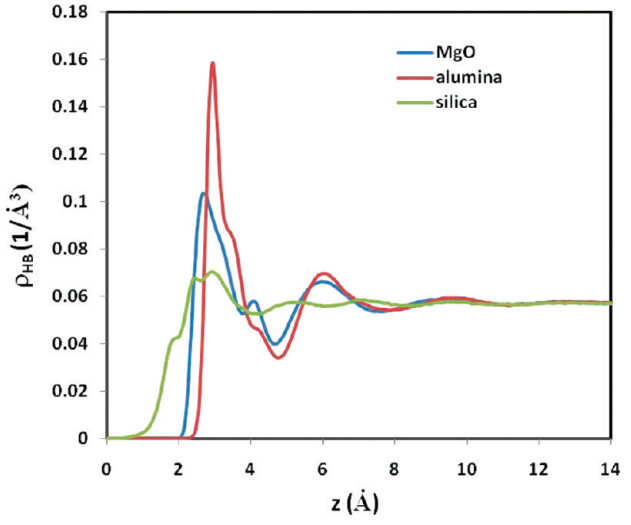

Figure 17. Density profiles of hydrogen bonds formed between water molecules as a function of the distance z from the nonvibrating MgO (blue), hydroxylated alumina (red), and hydroxylated silica (green).

shown for the three substrates. The HB density in the first hydration layer is the largest on alumina and the least on silica. The high water−water HB density, combined with the high atomic density (see Figure 13), is probably responsible for slowing down the dynamical properties of interfacial water molecules.

SUMMARY AND CONCLUSIONS

MD simulations were employed to study structure and dynamics of water molecules at contact with a flat MgO substrate. Water molecules were modeled using the SPC/E model, whereas the solid substrate was simulated using the CLAYFF force field. Two representations for the solid were employed. In the first, all surface atoms were maintained rigid, whereas in the second, they were allowed to vibrate. By computing the contact angle for droplets of 1000 water molecules, we observed that better agreement with experimental data is achieved when the solid atoms are maintained rigid. The results obtained for water within thin films supported on rigid versus vibrating MgO did not exhibit significant differences, except for the water orientation within the first hydration layer. The results discussed include atomic density profiles in the direction perpendicular to the surface, atomic density distribution along planes parallel to the substrate, HB networks, 2-D RDFs in the direction parallel to the substrate, and residence autocorrelation functions used to assess the average residence time for water at contact with the solid substrate. The results are also compared with those obtained previously for water supported on model silica and alumina substrates in an attempt to relate the properties of a solid substrate to those of the film of interfacial water supported by the substrate.

The results show a pronounced patterning of interfacial water, especially in the first hydration layer, on all three substrates considered. The distribution of solid atoms on the substrate determines the availability of preferential adsorption sites where water molecules reside. Depending on the surface arrangement of these preferential adsorption sites, the planar distribution of water molecules at the interface and the network of water−water HBs are established. These, in turn, determine how far the surfaces perturb the properties of interfacial water and affect the residence time of water molecules at contact with the solid substrates. Although complete experimental corroboration is still not possible, the simulation results presented here are valuable for understanding macroscopic phenomena including ions adsorption at interfaces and hydrodynamic properties in the earth subsurface.

AUTHOR INFORMATION

Corresponding Author

*E-mail: astriolo@ou.edu.

Notes

The authors declare no competing financial interest.

ACKNOWLEDGMENTS

Financial support to the Striolo group was provided by the U.S. Department of Energy, Office of Basic Energy Sciences, under contract number DE-SC0001902 (which supported TAH), and DE-SC0006901 (Division of Chemical Sciences, Geosciences and Biosciences) (which supported AP). Generous allocations of computing time were provided by the Oklahoma Supercomputer Center for Education and Research (OSCER) and by the National Energy Research Scientific Computing Center (NERSC). NERSC is supported by the Office of Science of the U.S. Department of Energy under contract no. DE-AC02-05CH11231. A.S. is grateful to Thanos Panagiotopoulos and Pablo Debenedetti of Princeton University, where he is currently spending his sabbatical. DRC was supported under

contract DE-SC0006878 provided by the U.S. Department of Energy, Office of Basic Energy Sciences (Division of Chemical Sciences, Geosciences and Biosciences).

REFERENCES

(1) Fornasiero, F.; Park, H. G.; Holt, J. K.; Stadermann, M.; Grigoropoulos, C. P.; Noy, A.; Bakajin, O. *Proc. Natl. Acad. Sci. U.S.A* **2008**, *105*, 17250.
(2) Hille, B. *Ion Channels of Excitable Membranes*, 3rd ed.; Sinauer Asscociates: Sunderland, MA, 2001.
(3) Jiang, Y.; Lee, A.; Chen, J.; Cadene, M.; Chait, B. T.; MacKinnon, R. *Nature* **2002**, *417*, 512.
(4) Argyris, D.; Cole, D. R.; Striolo, A. *ACS Nano* **2010**, *4*, 2035.
(5) Ho, T. A.; Argyris, D.; Cole, D. R.; Striolo, A. *Langmuir* **2012**, *28*, 1256.
(6) Striolo, A. *Adsorpt. Sci. Technol.* **2011**, *29*, 211.
(7) Gates, B. C. *Catalytic Chemistry*; John Wiley and Sons: New York, 1992.
(8) Henrich, V. E.; Cox, P. A. *The Surface Science of Metal Oxides*; Cambridge University Press: Cambridge, U.K., 1994.
(9) Greenland, D. J.; Hayes, M. H. B. *The Chemistry of Soil Constituents*; John Wiley and Sons: New York, 1978.
(10) Hochella, M. F.; White, A. F. *Mineral-Water Interface Geochemistry*; Mineralogical Society of America: Washington, DC, 1990.
(11) Spostio, G. *The Surface Chemisty of Soils*; Oxford University Press: Oxford, U.K., 1984.
(12) Stumm, W. *Chemistry of the Solid-Water Interface: Processes at the Mineral-Water and Particle-Water Interface in Natural Systems*; John Wiley and Sons: New York, 1992.
(13) Welton-Cook, M. R.; Prutton, M. *Surf. Sci.* **1978**, *74*, 276.
(14) Causa, M.; Dovesi, R.; Pisani, C.; Roetti, C. *Surf. Sci.* **1986**, *175*, 551.
(15) Martin, A. J.; Bilz, H. *Phys. Rev. B* **1979**, *19*, 6593.
(16) Urano, T.; Kanaji, T.; Kaburagi, M. *Surf. Sci.* **1983**, *134*, 109.
(17) Karolewski, M. A.; Cavell, R. G. *Surf. Sci.* **1992**, *271*, 128.
(18) Knozinger, E.; Jacob, K. H.; Singh, S.; Hofmann, P. *Surf. Sci.* **1993**, *290*, 388.
(19) Peng, X. D.; Barteau, M. A. *Surf. Sci.* **1990**, *233*, 283.
(20) Peng, X. D.; Barteau, M. A. *Langmuir* **1991**, *7*, 1426.
(21) Wu, M. C.; Estrada, C. A.; Corneille, J. S.; Goodman, D. W. *J. Chem. Phys.* **1992**, *96*, 3892.
(22) Wu, M. C.; Goodman, D. W. *Catal. Lett.* **1992**, *15*, 1.
(23) Langel, W.; Parrinello, M. *Phys. Rev. Lett.* **1994**, *73*, 504.
(24) Nada, R.; Hess, A. C.; Pisani, C. *Surf. Sci.* **1995**, *336*, 353.
(25) Picaud, S.; Hoang, P. N. M.; Girardet, C. *Surf. Sci.* **1992**, *278*, 339.
(26) Refson, K.; Wogelius, R. A.; Eraser, D. G.; Payne, M. C.; Lee, M. H.; Milman, V. *Phys. Rev. B* **1995**, *52*, 10823.
(27) Scamehorn, C. A.; Hess, C. A.; McCarthy, M. I. *J. Chem. Phys.* **1993**, *99*, 2786.
(28) Minot, C. *Surf. Sci.* **2004**, *562*, 237.
(29) McCarthy, M. I.; Schenter, G. K.; Scamehorn, C. A.; Nicholas, J. B. *J. Phys. Chem.* **1996**, *100*, 16989.
(30) Ho, T. A.; Argyris, D.; Papavassiliou, D. V.; Cole, D. R.; Striolo, A. *Mol. Simul.* **2011**, *37*, 172.
(31) Skelton, A. A.; Fenter, P.; Kubicki, J. D.; Wesolowski, D. J.; Cummings, P. T. *J. Phys. Chem. C* **2011**, *115*, 2076.
(32) Skelton, A. A.; Wesolowski, D. J.; Cummings, P. T. *Langmuir* **2011**, *27*, 8700.
(33) Cygan, R. T.; Liang, J. J.; Kalinichev, A. G. *J. Phys. Chem. B* **2004**, *108*, 1255.
(34) Argyris, D.; Ho, T. A.; Cole, D. R.; Striolo, A. *J. Phys. Chem. C* **2011**, *115*, 2038.
(35) Legg, K. O.; Prutton, M.; Kinniburgh, C. G. *J. Phys. C: Solid State Phys.* **1974**, *7*, 4236.
(36) Kinniburgh, C. G. *J. Phys. C: Solid State Phys.* **1975**, *8*, 2382.
(37) Kinniburgh, C. G. *J. Phys. C: Solid State Phys.* **1976**, *9*, 2695.
(38) Argyris, D.; Cole, D. R.; Striolo, A. *Langmuir* **2009**, *25*, 8025.
(39) Argyris, D.; Tummala, N. R.; Cole, D. R.; Striolo, A. *J. Phys. Chem. C* **2008**, *112*, 13587.
(40) Berendsen, H. J. C.; Grigera, J. R.; Straatsma, T. P. *J. Phys. Chem.* **1987**, *91*, 6269.
(41) Miyamoto, S. K., P. A. *J. Comput. Chem.* **1992**, *13*, 952.
(42) Allen, M. P.; Tildesley, D. J. *Computer Simualtion of Liquids*; Oxford University Press: Oxford, U.K., 2004.
(43) Essmann, U.; Perera, L.; Berkowitz, M. L.; Darden, T.; Lee, H.; Pedersen, L. G. *J. Chem. Phys.* **1995**, *103*, 8577.
(44) Hoover, W. G. *Phys. Rev. A* **1985**, *31*, 1695.
(45) Nose, S. *Mol. Phys.* **1984**, *52*, 255.
(46) Hess, B.; Kutzner, C.; Van der Spoel, D.; Lindahl, E. *J. Chem. Theory Comput.* **2008**, *4*, 435.
(47) Van der Spoel, D.; Lindahl, E.; Hess, B.; Groenhof, G.; Mark, A. E.; Berendsen, H. J. C. *J. Comput. Chem.* **2005**, *26*, 1701.
(48) Hockney, R. W.; Goel, S. P.; Eastwood, J. W. *J. Comput. Phys.* **1974**, *14*, 148.
(49) Tobbens, D. M.; Stusser, N.; Knorr, K.; Mayer, H. M.; Lampert, G. *Mater. Sci. Forum* **2001**, *378*−*3*, 288.
(50) Jamadagni, S. N.; Godawat, R.; Garde, S. *Langmuir* **2009**, *25*, 13092.
(51) McCarthy, T. J.; Gao, L. C. *Langmuir* **2008**, *24*, 9183.
(52) Bratko, D.; Wang, J. H.; Luzar, A. *Proc. Natl. Acad. Sci. U.S.A* **2011**, *108*, 6374.
(53) Ho, T. A.; Papavassiliou, D. V.; Lee, L. L.; Striolo, A. *Proc. Natl. Acad. Sci. U.S.A* **2011**, *108*, 16170.
(54) Giovambattista, N.; Debenedetti, P. G.; Rossky, P. J. *J. Phys. Chem. B* **2007**, *111*, 9581.
(55) Gonzalez-Martin, M. L.; Labajos-Broncano, L.; Janczuk, B.; Bruque, J. M. *J. Mater. Sci.* **1999**, *34*, 5923.
(56) Marti, J. *J. Chem. Phys.* **1999**, *110*, 6876.
(57) Chang, T.; Dang, L. X. *J. Chem. Phys.* **1996**, *104*, 6772.
(58) Wang, C. L.; Lu, H. J.; Wang, Z. G.; Xiu, P.; Zhou, B.; Zuo, G. H.; Wan, R. Z.; Hu, J. Z.; Fang, H. P. *Phys. Rev. Lett.* **2009**, *103*, 137801.
(59) Lutzenkirchen, J.; Zimmermann, R.; Preocanin, T.; Filby, A.; Kupcik, T.; Kuttner, D.; Abdelmonem, A.; Schild, D.; Rabung, T.; Plaschke, M.; Brandenstein, F.; Werner, C.; Geckeis, H. *Adv. Colloid Interface Sci.* **2010**, *157*, 61.
(60) Thomas, A. C.; Richardson, H. H. *J. Phys. Chem. C* **2008**, *112*, 20033.
(61) Giovambattista, N.; Debenedetti, P. G.; Rossky, P. J. *Proc. Natl. Acad. Sci. U.S.A* **2009**, *106*, 15181.